Plant Soil (2017) 414:33–51
DOI 10.1007/s11104-016-3089-5

REGULAR ARTICLE

Diel plant water use and competitive soil cation exchange interact to enhance NH_4^+ and K^+ availability in the rhizosphere

Javier F. Espeleta · Zoe G. Cardon · K. Ulrich Mayer · Rebecca B. Neumann

Received: 11 May 2016 / Accepted: 14 October 2016 / Published online: 12 November 2016

Abstract
Aims Hydro-biogeochemical processes in the rhizosphere regulate nutrient and water availability, and thus ecosystem productivity. We hypothesized that two such processes often neglected in rhizosphere models — diel plant water use and competitive cation exchange — could interact to enhance availability of K^+ and NH_4^+, both high-demand nutrients.
Methods A rhizosphere model with competitive cation exchange was used to investigate how diel plant water use (i.e., daytime transpiration coupled with no nighttime water use, with nighttime root water release, and with nighttime transpiration) affects competitive ion interactions and availability of K^+ and NH_4^+.
Results Competitive cation exchange enabled low-demand cations that accumulate against roots (Ca^{2+}, Mg^{2+}, Na^+) to desorb NH_4^+ and K^+ from soil, generating non-monotonic dissolved concentration profiles (i.e. 'hotspots' 0.1–1 cm from the root). Cation accumulation and competitive desorption increased with net root water uptake. Daytime transpiration rate controlled diel variation in NH_4^+ and K^+ aqueous mass, nighttime water use controlled spatial locations of 'hotspots', and day-to-night differences in water use controlled diel differences in 'hotspot' concentrations.
Conclusions Diel plant water use and competitive cation exchange enhanced NH_4^+ and K^+ availability and influenced rhizosphere concentration dynamics. Demonstrated responses have implications for understanding rhizosphere nutrient cycling and plant nutrient uptake.

Keywords Hydraulic redistribution · Nighttime transpiration · Plant nutrient uptake · Reactive-transport · Rhizosphere · Root water uptake

Responsible Editor: Ellis Hoffland.

Electronic supplementary material The online version of this article (doi:10.1007/s11104-016-3089-5) contains supplementary material, which is available to authorized users.

J. F. Espeleta · R. B. Neumann (✉)
Department of Civil and Environmental Engineering, Civil & Environmental Engineering, University of Washington, 201 More Hall, Box 352700, Seattle, WA 98195-2700, USA
e-mail: rbneum@uw.edu

Z. G. Cardon
The Ecosystems Center, Marine Biological Laboratory, 7 MBL Street, Woods Hole, MA 02543, USA

K. U. Mayer
Department of Earth, Ocean and Atmospheric Sciences, University of British Columbia, Vancouver, BC, Canada

Introduction

Plant roots and their associated soil environment (i.e., the rhizosphere) represent the belowground portion or 'hidden half' of ecosystems (Waisel et al. 1991). This 'hidden half' plays a crucial role in regulating ecosystem processes, affecting nutrient and water availability and thus ecosystem productivity (Chapin et al. 2002). Since the terrestrial biosphere strongly interacts with climate, for over a decade it has been recognized that an understanding of the physical, geochemical and biological processes occurring within this belowground

ecosystem is required to reduce uncertainty and improve predictions of climate change (Norby and Jackson 2000). Despite this recognition, knowledge gaps persist, driven, in part, by the fact that belowground ecosystems are difficult to observe and important processes occur at μm- to mm- spatial scales. Root-soil interactions, specifically, the coupled impact of hydrologic and biogeochemical processes on nutrient and carbon flow through roots and soil, have been identified as a persistent critical knowledge gap (Matamala and Stover 2013).

Given the difficulties of empirically studying μm- to mm-scale processes in the rhizosphere, computer models that simulate water flow and solute transport toward roots are one tool used to advance mechanistic understanding of root and rhizosphere processes that influence plant and soil microbiological behavior (Luster et al. 2009). Despite this need to understand coupled hydrologic and biogeochemical interactions in the rhizosphere, models often use simplified representations of hydrologic and geochemical processes. Instead of simulating diel plant water use (i.e., transpiration during the day and no water use during the night), a steady root-ward water flux is frequently imposed; instead of simulating competitive cation exchange, sorption interactions between dissolved nutrients and soil are often represented with a linear sorption isotherm or buffer coefficient, which implies that partitioning of a given ion between the aqueous and solid phase is independent of and unaffected by concentrations and partitioning behavior of other ions (e.g., Claassen et al. 1986; Barber 1995; Tinker and Nye 2000; Nowack et al. 2006; Lin and Kelly 2010). We hypothesized that these two often-neglected processes — diel plant water use and competitive cation exchange — could interact to alter nutrient availability and nutrient concentration patterns in the rhizosphere, with implications for understanding rhizosphere nutrient cycling and plant nutrient uptake.

Plant transpiration facilitates solute transport in the plant and through rhizosphere soil surrounding roots. A plant-facilitated increase in transpiration rate increases the mass-flow delivery rate of needed solutes to the root. Since mass-flow transports all soil solutes to the root, this delivery method can result in the accumulation of solutes next to the root for which the plant has a low demand, such as calcium (Ca^{2+}), magnesium (Mg^{2+}) and sodium (Na^{+}) (Lorenz et al. 1994; Tinker and Nye 2000; Nowack et al. 2006). Classically, solute accumulation next to the root is viewed as the simple outcome of solute delivery rates exceeding rates of plant uptake. However, we reasoned that when competitive soil cation exchange is accounted for, rhizosphere accumulation of low-demand cations (e.g., Ca^{2+}, Mg^{2+} and Na^{+}) could actually increase the availability of high-demand cations such as ammonium (NH_4^{+}) and potassium (K^{+}); the accumulated Ca^{2+}, Mg^{2+} and Na^{+} should outcompete NH_4^{+} and K^{+} for sorption sites, resulting in the release of NH_4^{+} and K^{+} from soil. Via this mechanism, a plant-facilitated increase in transpiration rate could not only increase mass-flow delivery of needed solutes, but also facilitate the release of needed nutrients, specifically NH_4^{+} and K^{+}, from the soil.

With this conceptualization, we further hypothesized that plant-driven water flow patterns would influence the temporal and spatial availability of NH_4^{+} and K^{+} in the rhizosphere. Diel oscillation in plant water use should shift the location of competitive cation exchange toward the root during the day when the plant is transpiring and there is root-ward solute transport. During the night, when the plant stops transpiring, the location of competitive cation exchange should shift further into the rhizosphere as accumulated solutes diffuse away from the root back into rhizosphere soil. Similarly, variations in nighttime plant water use, such as nighttime transpiration (Dawson et al. 2007) and nighttime water release facilitated by hydraulic redistribution (i.e., the passive movement of water from moist soil layers into dry soil layers through the root systems of plants; Caldwell and Richards 1989), could alter the net accumulation of low-demand cations against the root, influencing the magnitude of competitive cation displacement, and could alter the nighttime movement of accumulated cations back into the rhizosphere, influencing the location of NH_4^{+} and K^{+} displacement. Such spatial and temporal variability in rhizosphere resources influence both microbial and plant access to required nutrients (Cardon and Gage 2006).

These hypotheses build upon the results of a small set of previous rhizosphere and plant-uptake models that included competitive cation exchange (Bouldin 1989; Yakirevich et al. 1994; Nietfeld and Prenzel 2015). The first plant-uptake model that

included competitive soil cation exchange, developed by Bouldin in 1989, demonstrated that plant uptake of K^+ can increase as rhizosphere ion concentrations increase, given a low K^+ to [Ca^{2+} + Mg^{2+}] ratio on the soil exchanger. Similarly, modeling work by Yakirevich et al. (1994), which was focused on plant uptake of K^+ in saline soils, found that K^+ uptake increased as total cation exchange capacity (CEC) of the soil increased because near the root, Ca^{2+}, Mg^{2+} and Na^+ displaced K^+ off the soil exchanger, and as CEC increased, a larger amount of K^+ was sorbed to the exchanger and thus released into soil solution. Both of these previous models were predominately focused on plant uptake of cations and, thus, did not explore how the modeled processes impacted rhizosphere concentration patterns. In addition, both models simulated a constant root-ward water flow; diel variation in plant water use was not considered.

A more recent model with competitive cation exchange, developed by Nietfeld and Prenzel (2015) for plants growing in acidic soils, investigated how root-induced pH differences and aluminum dynamics altered both root uptake and rhizosphere concentration patterns of base cations. They simulated multiple scenarios, most of them with a constant root-ward water flow, and found that competitive desorption of base cations by aluminum ions at the root-soil interface increased aqueous concentrations of base cations within rhizosphere soil and enhanced root uptake of base cations, relative to simulations that did not include competitive exchange. Notably, the model produced concentration gradients in soil solution that were opposite to those on the soil exchanger, an outcome that is not possible to replicate with a sorption isotherm. One simulated scenario included diel plant water use (i.e., root-ward water flow during the day and no flow during the night). In this scenario, aqueous base cation concentrations at the root-soil interface and in the rhizosphere soil increased during the water flux period and decreased during the diffusion period. These diel concentration oscillations overlapped with more gradual concentration changes controlled by the evolution of the soil exchanger composition. This simulation was, to our knowledge, the first to couple competitive cation exchange with diel plant water use. However, the net effect of using a diel patterned water flux relative to a constant root-ward water flux on the availability of base cations within the rhizosphere was not discussed.

Collectively, this small set of models (Bouldin 1989; Yakirevich et al. 1994; Nietfeld and Prenzel 2015) demonstrated that competitive ion interactions in the rhizosphere can markedly affect the simulated availability of cations, particularly K^+, which is in high demand by the plant and has a weaker affinity for sorption sites relative to Ca^{2+} and Mg^{2+} (Appelo and Postma 2005). The one simulated scenario by Nietfeld and Prenzel (2015) that included diel plant water use showed that plant-driven flow oscillation generates temporal variability in cation concentrations, indicating an opportunity for plant-driven flow patterns to influence competitive ion interactions.

Adding to these previous modeling efforts, we developed a single-root model in MIN3P (Mayer et al. 2002), a process-based multicomponent reactive transport code, to simultaneously simulate unsaturated water flow, gas transport, solute transport, competitive soil cation exchange, and active root uptake of water and nutrients. Our goal was to examine the importance of competitive cation exchange in the rhizosphere and to advance understanding of how plant-driven flow patterns affect these competitive interactions and alter the availability of cations, specifically K^+ and NH_4^+. The previous competitive-cation exchange models (Bouldin 1989; Yakirevich et al. 1994; Nietfeld and Prenzel 2015) did not explicitly consider rhizosphere availability of NH_4^+, although NH_4^+ has a similar affinity as K^+ for sorption sites (Appelo and Postma 2005) and is also in high demand by the plant.

To test our hypotheses, we simulated multiple scenarios of diel plant water use, including daytime transpiration coupled with:

1. no plant water use during the night,
2. nighttime root water release, and
3. nighttime transpiration.

In addition we tested the impact of both high and low rates of daytime transpiration using the first scenario (i.e., no plant water use during the night). All of these simulated conditions mimicked patterns of plant water use in natural ecosystems (Coners and Leuschner 2005; Neumann and Cardon 2012; Forster 2014). To clarify the effect of diel plant water use and to compare our

results to previous studies, we also simulated a constant root-ward water flow condition.

Methods

Modeling approach

The multicomponent reactive-transport code MIN3P (MIN3P-THCm-X64 version 1.0.259.0) was used to develop a radial, one-dimensional, single-root model simulating the behavior of one root located in the center of a uniform radial soil domain and not influenced by neighboring roots. The MIN3P code is thoroughly described in Mayer et al. (2002). Briefly, it simulates unsaturated flow assuming an incompressible fluid, no hysteresis and a passive air phase, and using standard soil hydraulic functions following the formulation of Wösten and van Genuchten (1988). Reactive transport is simulated by simultaneously solving for advective transport and hydrodynamic dispersion (i.e., free-liquid diffusion plus mechanical dispersion) of dissolved species, diffusive gas transport, and user-defined geochemical reactions involving aqueous, gaseous and mineral species. Mass is conserved and electroneutrality is maintained in the reactive-transport solutions. Diffusive transport, in both the aqueous and gaseous phases, scales with porosity and soil moisture content according to the Millington-Quirk tortuosity expression (Millington and Quirk 1959). The mechanical dispersion coefficient (D_{mech}) scales with soil moisture (θ) according to : $D_{\mathrm{mech}} = \frac{\alpha q}{\theta}$, where α is dispersivity and q is the Darcy flux. The MIN3P code, including the radial formulation, has been thoroughly tested and benchmarked (Carrayrou et al. 2010; Mayer and MacQuarrie 2010; Marty et al. 2015; Rasouli et al. 2015; Steefel et al. 2015).

For this study, the included user-defined geochemical reactions were competitive cation exchange, aqueous complexation and gas dissolution-exsolution. Ion-exchange reactions in MIN3P can be described by the Vanselow, Gapon or Gaines-Thomas conventions (Appelo and Postma 2005). The approach assumes equilibrium between exchanged and dissolved concentrations for all cations and accounts for the fact that cations have different affinities for the solid phase. For the present simulations, the Gaines-Thomas model was employed and ion-exchange coefficients from the MINTEQA2 database (Allison et al. 1991) were used. Aqueous complexation in MIN3P is modeled as a reversible equilibrium reaction. Equilibrium coefficients for these reactions were similarly taken from the MINTEQA2 database. Gas exchange in MIN3P is modeled as an equilibrium reaction using Henry's law.

Modeled species

Given the focus on cations, the following components were defined in the rhizosphere model: H^+, NH_4^+, K^+, Ca^{2+}, Mg^{2+}, Na^+, NO_3^-, CO_3^{2-} and Cl^-. The anions CO_3^{2-} and Cl^- were included for charge balance and NO_3^- was included as a reference non-sorbing nutrient. In addition, CO_2 gas was included, as were the following secondary aqueous species: OH^-, $NH_{3(aq)}$, $MgOH^+$, $MgCO_{3(aq)}$, $MgHCO_3^+$, $CaOH^+$, $CaHCO_3^+$, $CaCO_{3(aq)}$, $NaCO_3^-$, $NaHCO_{3(aq)}$, HCO_3^-, $H_2CO_{3(aq)}$; and following sorbed species: NH_4-X, K-X, Ca-X_2, Mg-X_2, Na-X and H-X.

Rhizosphere domain

MIN3P uses a finite volume method for spatial discretization (Mayer et al. 2002). The soil domain extended from a radius of 0.01 cm where the root-soil boundary was placed, out to a radius of 10 cm where the bulk soil boundary was placed. The soil domain was discretized such that there was a finer spatial resolution with increasing proximity to the root-soil boundary. A fine spatial resolution was also established next to the outer bulk-soil boundary to assist with flux calculations across the boundary. Specifically, there were 13 equally spaced control volumes between a radius of 0.01 cm and 0.03 cm, and 20 equally spaced control volumes within each of the following seven radial intervals: 0.03–0.1 cm, 0.1–0.3 cm, 0.3–1 cm, 1–2.5 cm, 2.5–5 cm, 5–9 cm, 9–10 cm. Thus, there were a total of 153 control volumes. The domain consisted of a loam soil (UNSODA database, sensu Schaap and Leij 2000) with the physical and chemical properties described in Table 1. Water retention and unsaturated conductivity curves for the loam soil are presented in Supplemental Information Fig. S1. The cation exchange capacity (CEC) of the soil was estimated based on the percent clay and percent organic carbon typically found in loam soils (Table 1) and was kept constant during all model runs. Dispersivity was set to 0.1 cm (Table 1). Gelhar et al. (1992) demonstrated that dispersivity changes with and is often one to two orders of magnitude smaller than the spatial extent of the considered system.

Table 1 Input parameters

Input parameters	Value		Data source	Sensitivity test	
				low	high
Soil properties					
Cation exchange capacity (CEC) *	20	meq 100 g^{-1}	Appelo & Postma (2005)	*CEC* test [a]	
			Schaap & Leij (2000), Balland et al. (2008)	10	30
Bulk density †	1.3	g cm^{-3}	Brady & Weil (2002), Schaap & Leij (2000)		
van Genuchten parameters (loam)			UNSODA database (Schaap & Leij 2000)		
α	4.07	m^{-1}			
n	1.19				
Saturated soil moisture (Porosity)	0.51	m^3 m^{-3}			
Residual moisture content	0.06	m^3 m^{-3}			
Saturated hydraulic conductivity	3.04E-06	m s^{-1}			
Tortuosity parameter	-6.97				
Specific storage coefficient	9.83E-04		Domenico & Schwartz (1998)		
Aqueous diffusion coefficient	2.2E-09	m^2 s^{-1}	SI Table S5		
Gaseous diffusion coefficient	2.0E-05	m^2 s^{-1}	Marrero & Mason (1972)		
Longitudinal dispersivity	1.00E-03	m	Gelhar et al. (1992), Tinker & Nye (2000)		
Soil solution concentration (initial and bulk soil)				C_t Ratio Test [b]	
NO_3^-	1.7E-01	mmol L^{-1}	Median of 26 soils from 5 sites, SI Table S3	1.5E-01	3.7E-01
$NH4^+$	1.9E-02	mmol L^{-1}		4.8E-02	1.1E-02
K^+	5.4E-02	mmol L^{-1}		9.3E-02	8.6E-02
Ca^{+2}	1.9E-01	mmol L^{-1}		1.3E-01	1.9E-01
Mg^{+2}	7.8E-02	mmol L^{-1}		1.0E-01	6.1E-02
Na^+	1.6E-01	mmol L^{-1}		1.6E-01	1.5E-01
Cl^- (calculated for electroneutrality)	4.1E-04	mmol L^{-1}		3.9E-01	2.5E-01
HCO_3^-	1.6E-01	mmol L^{-1}		2.2E-01	1.4E-01
DIC (calculated from HCO_3^- and pH)	5.2E-01	mmol L^{-1}		7.3E-01	4.6E-01
pCO_2 (g) (calculated by MIN3P)	1.08	%			
pH (set)	6.0				
Root properties					
Nutrient Uptake Kinetics Test					
V_{max}				V_{max} Test [c]	
NO_3^-	2.32E-07	mol cm^{-2} h^{-1}	Median value from literature, SI Table S4	1.93E-06	1.59E-05
$NH4^+$	3.60E-07			3.00E-06	2.38E-05
K^+	1.31E-07			1.70E-06	4.45E-06
Ca^{+2}	6.37E-09			1.18E-07	1.00E-06
Mg^{+2}	4.40E-09			6.25E-08	1.53E-06
Na^+	6.07E-11			4.49E-10	1.16E-06
Cl^-	1.59E-11			4.42E-10	5.08E-10
K_m				K_m Test [c]	
NO_3^-	1.34E-04	mol cm^{-3}	Median value from literature, SI Table S4	281.8	61.9
$NH4^+$	5.39E-05			180.4	42.0
K^+	2.34E-05			31.0	15.5
Ca^{+2}	6.32E-05			77.0	33.1
Mg^{+2}	1.24E-05			38.1	9.5
Na^+	6.60E-04			5.81E+04	137.3
Cl^-	1.40E-05			46.0	14.0

* CEC = [7*(% clay) + 35*(% C)]/10 (Breeuwsma et al. 1986)

% clay =24.5 %; mid-range clay content of loam soils from soil texture triangle (sensu Schaap and Leij 2000)

% C = (% OM)*0.58; carbon content of organic matter (sensu Breeuwsma et al. 1986)

% OM = 1.4 %; mean soil organic matter content from UNSODA database (n = 459, Balland et al. 2008)

† Bulk density = (1 - n)*particle density (Brady and Weil 2002)

n = 0.51, mean porosity of UNSODA soils (sensu Schaap and Leij 2000)

Soil particle density = 2.65 g cm-3 (Brady and Weil 2002)

[a]: CEC limits were calculated with the minimum (7 %) and and maximum (40 %) clay content of loam soils (Schaap and Leij 2000)

[b]: Limits for concentration ratios were calculated relative to $NH4^+$ using the first and third quartile of $NH4^+$-to-ion ratios from 26 soil solution samples (SI Table S3)

[c]: Limits for root uptake kinetics were based on the first and third quartile of kinetic parameters from published studies (SI Table S4)

In our model, the scale of interest ranged between 1 cm and 10 cm; concentration profiles changed over a 1 cm radial distance (see Fig. 2) and the modeled domain was 10-cm long. Further, the chosen dispersivity value aligned with those reported and used by Tinker and Nye (2000) for plant and root-scale systems. Values for other needed soil property and solute transport parameters are listed in Table 1.

Boundary conditions – unsaturated flow

A constant water potential of −0.5 MPa was prescribed at the bulk-soil boundary (Ψ_{sb}) and a time-varying water potential was prescribed at the root-soil interface (Ψ_{sr}), mimicking daily oscillations in soil water potential measured in natural ecosystems (e.g., Meinzer et al. 2004; Cardon et al. 2013) and establishing unsaturated, diel water-flow across the soil domain. This approach assumes no competition for water between neighboring roots and captures flow conditions with the bulk soil water potential poised at an ecologically relevant point. Specifically, at a soil water potential of −0.5 MPa, empirical studies have detected both nighttime transpiration and nighttime root water release facilitated by hydraulic redistribution (HR). Nighttime transpiration is a phenomenon that occurs when soils are moist and decreases in magnitude as soils dry (Dawson et al. 2007; Neumann et al. 2014). In an experiment conducted with sunflower, nighttime transpiration occurred when soil water potentials were above −1 MPa (Neumann et al. 2014). Upward HR occurs when surface soils dry and deeper soils remain moist. The soil water potential difference between soil layers drives flow through the root system from the moist soil layer into the dry soil layer. In multiple different studies, upward HR began when surface soils dried to −0.4 to −0.8 MPa (Ishikawa and Bledsoe 2000; Domec et al. 2004; Meinzer et al. 2004).

Six different 24-h time courses of root water potentials were created to simulate:

1) daytime transpiration coupled with nighttime cessation of plant water uptake (Base Case scenario),
2) a two-times slower rate of daytime transpiration coupled with nighttime cessation of plant water uptake,
3) a two-times faster rate of daytime transpiration coupled with nighttime cessation of plant water uptake,
4) daytime transpiration coupled with nighttime root water release,
5) daytime transpiration coupled with a slower rate of nighttime transpiration, and
6) continuous daytime and nighttime transpiration generating a constant root-ward water flux.

The daytime period was 14 h long and the nighttime period was 10 h long. These 24-h time courses were repeated everyday for the length of the simulation.

For the first three scenarios, during the day, Ψ_{sr} followed a positive hyperbolic curve that started and ended at the bulk-soil water potential (Ψ_{sb}), and reached a minimum water-potential value in the middle of the daytime period (Fig. 1a, lines c–e). During the nighttime period, Ψ_{sr} matched Ψ_{sb} (Fig. 1a, lines c–e). For the fourth scenario, the daytime transpiration curve matched that of the base-case scenario and nighttime root-water release was simulated with a negative hyperbolic curve that peaked in the middle of the nighttime period with Ψ_{sr} exceeding that of Ψ_{sb} (Fig. 1b, line f). For the fifth scenario, the root water-potential time series was similar to that for the base-case scenario, except to simulate nighttime transpiration, Ψ_{sr} never reached Ψ_{sb} (Fig. 1b, line g). For the sixth scenario, a hypothetical scenario with constant root-ward water flow, the root water potential was set to a constant value of −0.6 MPa (Fig. 1b, line h). The equation for a hyperbolic curve is:

$$y = k \pm \alpha\sqrt{1 + \frac{(t-h)^2}{b^2}},$$

where y is the root-soil water potential (MPa), t is time (day), and a (MPa), b (day), k (MPa) and h (day) are parameters for the curve describing its shape and location with the t-y domain. Values for a, b, k and h are presented in SI Table S1 for each simulation that utilized a hyperbolic curve.

Water-potential distributions in the rhizosphere resulting from these described boundary conditions are presented in Figs. 1c–h, and simulated rates of root water uptake and water fluxes across the bulk soil boundary for the six scenarios are presented in SI Table S2. The simulated rates of root water uptake align with those measured, on a per root-length basis, for Douglas Fir and Western Hemlock growing in similarly moist soil conditions (Meinzer et al. 2007). Further, for the fourth scenario, the simulated rate of nighttime root-water

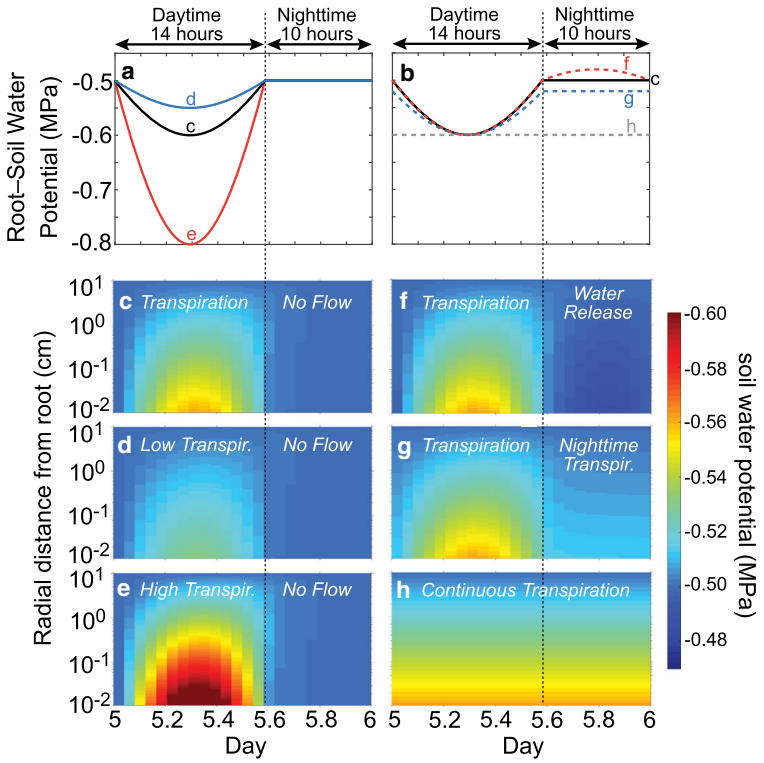

Fig. 1 Prescribed water potentials at root–soil boundary (Ψ_{sr}) for the six tested plant water use scenarios (**a**-**b**), and resulting soil water potentials in the rhizosphere domain (**c**-**h**) during day 5 of the simulation. Note log scale for radial distance from root in (**c**-**h**). The prescribed Ψ_{sr} curves in (**a**-**b**) were repeated every 24 h for the length of the simulation and designed to mimic different plant water use patterns: different rates of daytime transpiration coupled with no plant water use during the night (Ψ_{sr} curves c-e in (**a**) and soil water potential responses in (**c**-**e**)); daytime transpiration coupled with nighttime root water release (Ψ_{sr} curve f in (**b**) and soil water potential response in (**f**)); daytime transpiration coupled with nighttime transpiration (Ψ_{sr} curve g in (**b**) and soil water potential response in (**g**)); and constant root-ward water flow (Ψ_{sr} curve h in (**b**) and soil water potential response in (**h**))

release was 20 % of that taken up by the root during the day (SI Table S2), which aligns with the upper end of water release-to-uptake ratios from published HR field studies (Neumann and Cardon 2012), and for the fifth scenario, the simulated rate of nighttime transpiration was 20 % of the daytime transpiration rate (SI Table S2), which aligns with the 75th percentile of median nighttime to daytime transpiration ratios found in various ecosystems from temperate and tropical regions (Forster 2014).

Boundary conditions – reactive transport

A third-type (i.e., Cauchy) boundary condition was set at the bulk-soil boundary. This condition sets concentrations on a dummy node outside of the domain and chemicals flux into the domain based on simulated flow rates and concentrations inside the domain. The boundary acts as a free exit boundary when fluxes leave the domain. Concentrations on the dummy node corresponded to values representing median cation, nitrate and bicarbonate concentrations measured in natural soils, with pH set to 6.0 and Cl^- concentrations calculated to balance charge (Table 1 and SI Table S3).

The root-soil boundary was closed to passive chemical transport; dissolved and gaseous species could not advect or diffuse across the boundary. Root nutrient uptake was modeled for NH_4^+, K^+, Ca^{2+}, Mg^{2+}, Na^+, NO_3^- and Cl^- as an active process following Michaelis-Menten kinetics:

$$V = V_{\max}\frac{C}{K_m + C},$$

where V is the effective rate of nutrient uptake, C is the soil solute concentration adjacent to the root, V_{max} is the maximum uptake rate, and K_m is the substrate affinity constant which indicates the concentration at which V equals half of V_{max}. To maintain charge balance, uptake of cations (NH_4^+, K^+, Ca^{2+}, Mg^{2+}, Na^+) was

accompanied by the charge-equivalent release of H^+ at the root-soil boundary, and uptake of anions (NO_3^-, Cl^-) was accompanied by the charge-equivalent release of HCO_3^- at the root-soil boundary (Marschner 1995; Tinker and Nye 2000). Values for V_{max} and K_m (Table 1) were obtained from a literature search of studies measuring net uptake (uptake minus release) of modeled solutes by a range of different plants (SI Table S4).

Initial conditions

In the rhizosphere domain, for all simulations, the initial soil water potential was set to match that of the bulk soil boundary (−0.5 MPa) and initial soil solute concentrations were set to match those assigned to the dummy node outside of the bulk soil boundary (i.e., median concentrations found in natural soils with pH set to 6.0 and Cl^- concentrations calculated to balance charge, Table 1 and SI Table S3). Given these inputs, MIN3P used Henry's Law to calculate the partial pressure of CO_2 in the gas phase (PCO_2). The calculated PCO_2 was 1 % (Table 1), which aligns with measurements of PCO_2 in global soils (Brook et al. 1983). MIN3P includes an option, which was used, that determines the initial soil exchanger composition based on the given solution composition and the specified cation exchange capacity, without changing dissolved concentrations.

Sensitivity analysis

In addition to simulating different plant-driven flow conditions, we also tested the sensitivity of modeled nutrient profiles to variations in cation exchange capacity, root uptake kinetics, and cation concentration ratios using the value ranges shown in Table 1. Sensitivity to CEC was tested at three CEC levels defined by the minimum and maximum clay contents of loam soils and the empirical formula presented in Breeuwsma et al. (1986) (Table 1). A simulation with CEC = 0 was also added for comparison. The impact of nutrient uptake kinetics was tested two different ways. In the first test, Michaelis-Menten kinetic parameters for root uptake of just the low-demand cations (Ca^{2+}, Mg^{2+}, Na^+) were altered. In the second test, the kinetic parameters for root uptake of all ions (NO_3^-, NH_4^+, K^+, Ca^{2+}, Mg^{2+}, Na^+ and Cl^-) were altered. Slow root nutrient uptake was simulated with a large K_m (low substrate affinity) and small V_{max} (slow maximum rate of uptake), and fast root nutrient uptake was simulated with a small K_m (high affinity) and large V_{max} (fast maximum rate of uptake). Small and large parameter values corresponded, respectively, to the first and third quartiles from the range of values collected from the literature for a wide variety of plants (Table 1 and SI Table S4). Sensitivity to cation concentration ratio was tested with NH_4^+ as the focal cation (Table 1). Total cation concentration was kept constant, but the concentration ratio between each simulated cation and NH_4^+ was increased and decreased based on the first and third quartile of NH_4^+ concentration ratios reported in the literature for natural soils (SI Table S3).

Linear sorption comparison

One simulation was run using a linear sorption isotherm for NH_4^+ instead of competitive cation exchange. A K_d value of 0.8 mL/g was used (Jellali et al. 2010), resulting in a retardation factor of 3 given the bulk density and porosity values listed in Table 1.

Simulated time period

After initialization, simulations were run for a period of 30 days. Results focus on day 5. Five days was long enough to establish a consistent diel pattern in modeled nutrient profiles (see Movie 1 and Fig. 7) without developing extreme concentration build up or depletion near the root.

Results

Rhizosphere concentration profiles — base case scenario

Diel plant water use (i.e., transpiration-driven flow during the day and no plant water use during the night) coupled with root nutrient uptake and soil cation exchange resulted in the accumulation of dissolved Ca^{2+}, Mg^{2+} and Na^+ (all low-demand plant nutrients) and the depletion of dissolved NO_3^- (a high demand nutrient) within a 1-cm distance next to the root (Fig. 2a,e). Accumulation of Ca^{2+}, Mg^{2+} and Na^+ was greatest during the daytime period as transpiration driven flow delivered solutes to the root (Fig. 2a). During the nighttime period, Ca^{2+}, Mg^{2+} and Na^+ concentrations decreased, as did NO_3^- concentrations (Fig. 2e), as root-ward water flow ceased but the root continued to take up solutes (SI Fig. S2). pH

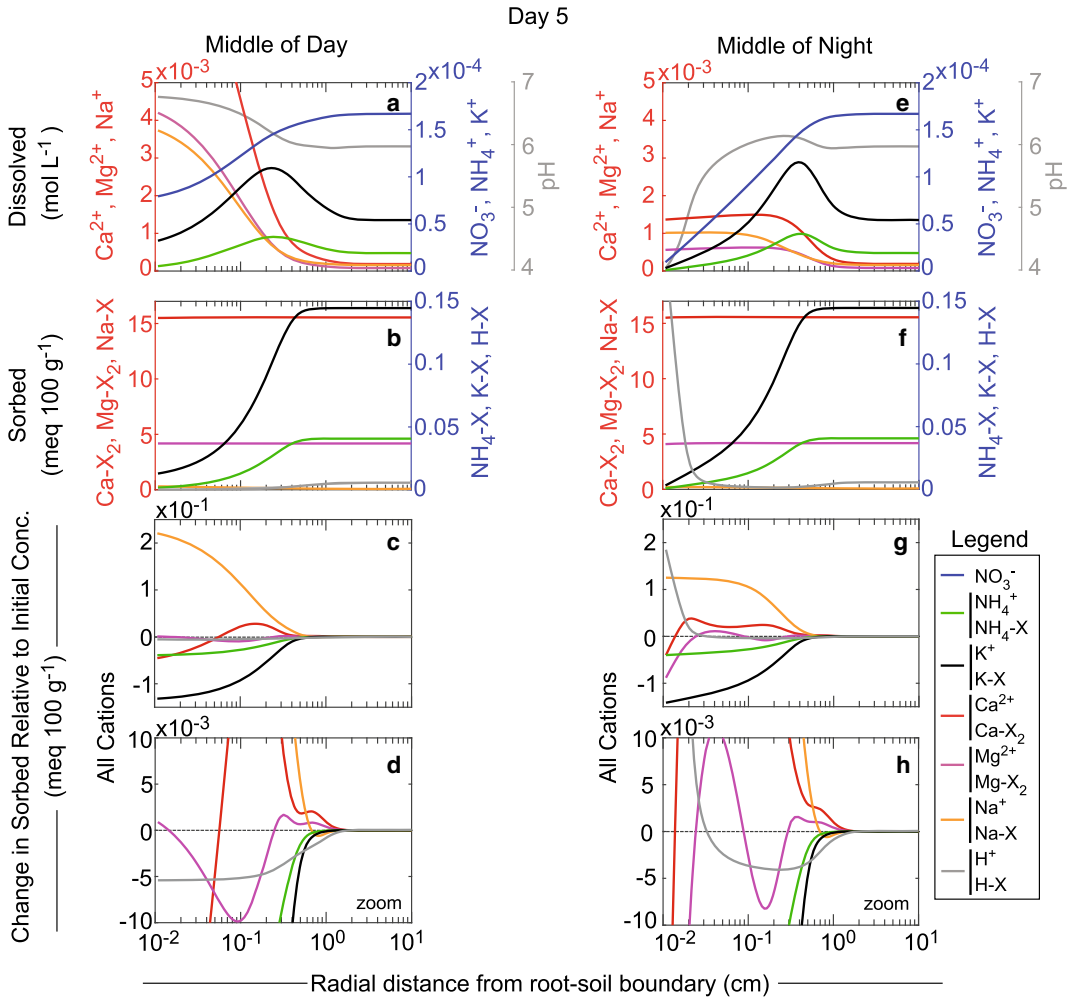

Fig. 2 Dissolved concentration profiles (**a**, **e**), sorbed concentration profiles (**b**,**f**), and changes in sorbed concentrations relative to initial conditions (**c**-**d**, **g**-**h**) for multiple ions on day 5 of the Base Case scenario. Profiles correspond with the middle of the daytime period (**a**-**d**) and middle of the nighttime period (**e**-**h**). Note log scale for radial distance from root

slightly increased next to the root during the day and dramatically decreased during the night in response to H^+ and HCO_3^- released by the root with the uptake of cations and anions, respectively, and loss of dissolved inorganic carbon to the gaseous phase (Fig. 2a,e; SI Fig. S2). The nighttime decrease in pH was driven by a larger uptake of cations than anions, and therefore a greater root release of H^+ than HCO_3^- during this period (SI Fig. S2). In contrast to Ca^{2+}, Mg^{2+}, Na^+, H^+ and NO_3^-, dissolved NH_4^+ and K^+, both positively charged high-demand nutrients, did not show uniform depletion towards the root. These two solutes developed concentration peaks (i.e., hotspots) at distances of 0.1–1 cm from the root that persisted day and night (Fig. 2a,e). Development of a non-monotonic concentration profile was not replicated with a linear sorption isotherm (SI Fig. S3), demonstrating that these concentration peaks were a result of competitive ion exchange.

On the soil exchanger, NH_4^+ and K^+ concentrations were depleted near the root due to competitive displacement by Ca^{2+}, Mg^{2+} and Na^+ (Fig. 2b,f). Movie 1 documents this displacement and shows that there was daily growth in the spatial extent of NH_4^+ and K^+ depletion zones on the soil exchanger, with most displacement occurring during the daytime period when dissolved Ca^{2+}, Mg^{2+} and Na^+ accumulated next to the root. Comparison of dissolved and sorbed profiles, both in Movie 1 and Fig. 2, indicates that peak dissolved NH_4^+ and K^+ concentrations were spatially

aligned with the outer edge of NH_4^+ and K^+ depletion zones on the soil exchanger where sorbed NH_4^+ and K^+ concentrations were largest. At this location, tail concentrations of dissolved Ca^{2+}, Mg^{2+} and Na^+ accumulation profiles actively displaced NH_4^+ and K^+ from the soil exchanger (Fig. 2 c,d,g,h). Calcium, magnesium and sodium were all involved with competitive displacement of NH_4^+ and K^+ from the soil exchanger. Figures 2c–h show that sorbed concentrations for all three of these low-demand cations experienced increases in locations where sorbed concentrations for NH_4^+ and K^+ decreased.

The shape, concentration and spatial location of the non-monotonic dissolved NH_4^+ and K^+ profiles were temporally dynamic due to diel plant water use. During the day, accumulation of Ca^{2+}, Mg^{2+} and Na^+ displaced NH_4^+ and K^+ from the soil exchanger and root-ward water flow transported this displaced NH_4^+ and K^+ toward the root, generating spatially wide dissolved concentration peaks (Movie 1; Fig. 2a). During the night, when root water uptake initially ceased, backward diffusion of Ca^{2+}, Mg^{2+} and Na^+ into the rhizosphere domain displaced a smaller amount of NH_4^+ and K^+ from the soil exchanger radially further from the root (i.e., compare radial location of plotted changes in sorbed concentrations in Fig. 2d and h) while root uptake of NH_4^+ and K^+ reduced dissolved concentrations of NH_4^+ and K^+ near the root, sharpening the dissolved NH_4^+ and K^+ concentration profiles and moving peak concentrations radially further into the rhizosphere domain (Movie 1; Fig. 2e). However, later in the nighttime period, continued diffusive transport of NH_4^+ and K^+ decreased peak concentrations, flattening out the dissolved concentration profiles (Movie 1).

These temporal dynamics in the shape, concentration and spatial location of the dissolved NH_4^+ and K^+ profiles did not occur with a constant root-ward water flow. With constant root-ward water flow, continued accumulation of Ca^{2+}, Mg^{2+} and Na^+ against the root over multiple days increased the radial extent for competitive displacement of NH_4^+ and K^+, slowly increasing dissolved NH_4^+ and K^+ concentrations and pushing the location of the concentration peaks radially further from the root (Movie 2). A similar longer-term concentration increase and peak-location shift also occurred with diel plant water use, but with the diel changes described above overlaid on top of these more gradual shifts in concentration and peak location (Movie 1).

Sensitivity tests

Peak concentrations of dissolved NH_4^+ and K^+ were sensitive to soil and plant-driven properties. The tested properties and values are listed in Table 1. For soil properties, peak concentrations of both dissolved NH_4^+ and K^+ increased as cation exchange capacity (CEC) increased (Fig. 3a; SI Fig. S4a), and peak concentration of dissolved NH_4^+ increased as the cation-to-NH_4^+ concentration ratio decreased (i.e., there was proportionately more NH_4^+ in the soil solution relative to other cations) (Fig. 3b). In agreement with the simulation that used a linear sorption isotherm (SI Fig. S3), at zero CEC, the NH_4^+ and K^+ hotspots disappeared completely (Fig. 3a; SI Fig. S4a). The simulated changes in the cation-to-NH_4^+ concentration ratio had a notably larger impact on the dissolved NH_4^+ concentration profile than did the simulated changes in CEC (Fig. 3a,b; note the different y-axis values). Fig. S4a shows the response of the dissolved K^+ concentration profile to changes in the cation-to-NH_4^+ concentration ratio. Dissolved K^+ concentrations increased both when the cation-to-NH_4^+ concentration ratio increased and when it decreased. This response is explained by the fact that the cation-to-K^+ concentration ratio decreased with respect to Ca^{2+}, Mg^{2+} and Na^+ both when the cation-to-NH_4^+ ratio increased and when it decreased (Table 1 and SI Table S3).

For plant-driven properties, changes in the Michaelis-Menten kinetic parameters for root nutrient uptake had minimal influence on dissolved NH_4^+ and K^+ profiles. The first tested scenario was a change in the kinetic parameters for just the low-demand cations (Ca^{2+}, Mg^{2+} and Na^+) involved with competitive displacement of NH_4^+ and K^+ from the soil exchanger. The dissolved NH_4^+ and K^+ profiles had no sensitivity to this change (Fig. 3c; SI Fig. S4c). Figs. S5 and S6 in Supplemental Information provide insight into this result. Fig. S5 plots net influx, sorption/desorption, gas dissolution/exsolution, root uptake/release and change in aqueous mass for all simulated ions over a 24-h period for both the Base Case scenario and the scenario with faster kinetic parameters for root uptake of Ca^{2+}, Mg^{2+} and Na^+. It shows that as the root took up more Ca^{2+}, Mg^{2+} and Na^+, more H^+ was released into the rhizosphere. H^+ reached a high enough concentration that it competitively displaced Ca^{2+}, Mg^{2+} and Na^+ from the soil exchanger; NH_4^+ and K^+ were not displaced in an appreciable amount because sorbed concentrations of

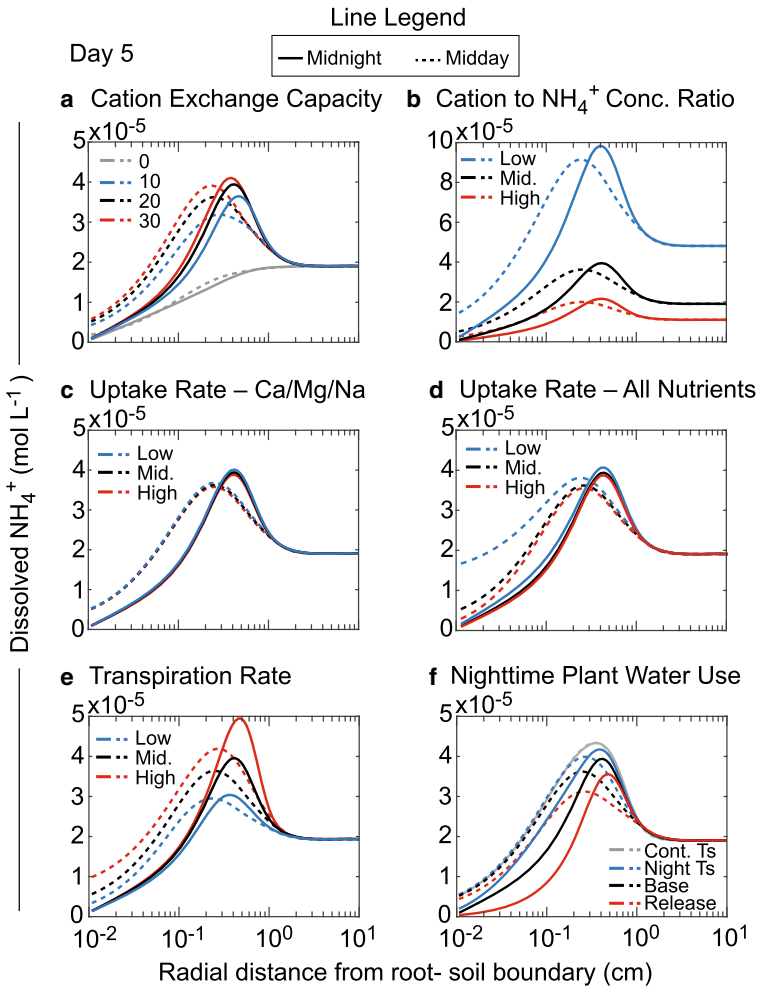

Fig. 3 Sensitivity of dissolved $NH4^+$ concentration profiles to variation in: (**a**) cation exchange capacity, (**b**) concentration ratio between other cations and $NH4^+$, with a low ratio representing proportionately more NH_4^+ relative to other cations, (**c**) kinetic parameters for root uptake of Ca^{2+}, Mg^{2+} and Na^+, (**d**) kinetic parameters for root uptake of all simulated ions, (**e**) daytime transpiration rate, and (f) nighttime plant water use. All variations were relative to the Base Case scenario. Solid lines are profiles are from the middle of the nighttime period and dashed lines are profiles from the middle of the daytime period

NH_4^+ and K^+ were low near the root (Fig. 2b,f). Competitive displacement of Ca^{2+}, Mg^{2+} and Na^+ from the soil exchanger by H^+ offset the faster rate of root uptake such that there was minimal difference between the two scenarios in aqueous mass for all of the simulated ions (SI Fig. S5), and therefore no change in the dissolved NH_4^+ and K^+ profiles (Fig. 3c, SI Fig. S4c). With slower root-uptake kinetic parameters for Ca^{2+}, Mg^{2+} and Na^+, aqueous mass of these low-demand cations slightly increased, but these changes altered sorption/desorption amounts for Ca^{2+} and H^+, rather than NH_4^+ and K^+ (SI Fig. S6).

The second tested scenario was a change in the kinetic parameters for root uptake of all simulated ions. The dissolved NH_4^+ and K^+ profiles had some sensitivity to this change. Faster root nutrient uptake kinetic parameters resulted in a very slight decrease in dissolved NH_4^+ and K^+ concentrations, while slower root nutrient uptake kinetic parameters resulted in a more appreciable increase in dissolved NH_4^+ and K^+ concentrations, particularly near the root during the day (Fig. 3d; SI Fig. S4d). The concentration increase was greater for K^+ than for NH_4^+ (Fig. 3d; SI Fig. S4d). These responses indicate that the rate of root uptake for NH_4^+ and K^+ in the Base Case scenario was already faster than the rate of delivery of these two solutes to the root. Faster kinetic parameters for NH_4^+ and K^+ root uptake did not alter actual rates of NH_4^+ and K^+ root uptake (SI Fig. S7), indicating transport limitation, and thus, this change had a minimal impact on dissolved NH_4^+ and K^+ concentrations. However, when slower kinetic parameters for NH_4^+ and K^+ root uptake were used, root uptake rates did decrease (SI Fig. S8) and the rate of NH_4^+ and K^+ delivery to the root during the day began to exceed the rate of root uptake, resulting in concentration increases near the root (Fig. 3d, SI Fig. S4d). Potassium

had a slower rate of root uptake than NH_4^+ (Table 1), explaining the larger increase in dissolved K^+ concentrations than in dissolved NH_4^+ concentrations.

With respect to plant-driven properties, the dissolved NH_4^+ and K^+ profiles were more sensitive to root water uptake than to root nutrient uptake. Peak concentrations of dissolved NH_4^+ and K^+ increased and decreased, both day and night, with an increase and decrease, respectively, in the rate of daytime transpiration when coupled with no plant water use during the night (Fig. 3e; SI Fig. S4e). Potassium accumulated against the root during the day with the increased transpiration rate (SI Fig. S4e), indicating that in this simulation, the daytime rate of K^+ delivery to the root exceeded the rate of K^+ root uptake. Variation in the nighttime flow pattern altered both concentrations and radial locations of the dissolved NH_4^+ and K^+ profiles. Root-ward water flow during the nighttime period increased peak concentrations and pushed peaks radially closer to the root, while nighttime water release by the root decreased peak concentrations and pushed peaks radially further from the root (Fig. 3f; SI Fig. S4f).

Effect of plant water use

The six tested plant-driven water-flow scenarios varied with respect to net amount of water taken up by the root during a 24-h period and in the difference between the amount of water taken up by the root during the daytime versus the nighttime periods. Figures 4–7 demonstrate how these variations across the flow scenarios influenced NH_4^+ and K^+ availability in the rhizosphere as well as peak concentrations for the dissolved NH_4^+ and K^+ profiles. Figure 4 shows that net root water uptake over a 24-h period controlled total availability of NH_4^+ and K^+ mass in the rhizosphere. Mass influx of NH_4^+ and K^+ into the domain, desorption of NH_4^+ and K^+, and root uptake of NH_4^+ and K^+ all increased as net root water uptake increased (Fig. 4a, c). Increased mass influx of NH_4^+ and K^+ with increased root water uptake was simply due to increased root-ward water flow transporting more solute mass into the domain. Increased desorption of NH_4^+ and K^+ with increased root water uptake was due to greater total cation transport into the domain promoting greater competitive displacement of NH_4^+ and K^+ (SI Fig. S9). With more NH_4^+ and K^+ mass transported into the domain and desorbed from the soil exchanger, root uptake of NH_4^+ and K^+ increased. However, net root water uptake, and thus total availability of NH_4^+ and K^+ in the domain, did not fully explain differences in total aqueous mass of NH_4^+ and K^+ across the flow scenarios (Fig. 4b, d), nor differences in concentrations of the dissolved NH_4^+ and K^+ peaks (at midnight; SI Fig. S10).

Figure 5 shows changes in the net influx, desorption, root uptake and aqueous mass of NH_4^+ over a 24-h period for the five different water-flow scenarios that simulated diel plant water use. A similar time course for K^+ is presented in SI Fig. S11. Results for the scenario with constant root-ward water flow are presented for both NH_4^+ and K^+ in SI Fig. S12. With regards to aqueous mass, the figures demonstrate that an increase in the daytime transpiration rate, when coupled with no plant water use during the night, enhanced diel variation in aqueous mass of both NH_4^+ and K^+ by reducing aqueous mass more during the daytime period and increasing aqueous mass more during the nighttime period, relative to the Base Case simulation (Fig. 5a,b; SI Fig. S11a,b). This variation is explained by the fact that a faster daytime transpiration rate promoted greater root uptake of NH_4^+ and K^+ during the daytime period and facilitated continued desorption of NH_4^+ and K^+ during the nighttime period. Similarly, a decrease in the daytime transpiration rate diminished diel variation in aqueous mass; less root uptake of NH_4^+ and K^+ occurred during the daytime period and minimal amounts of NH_4^+ and K^+ were desorbed during the nighttime period (Fig. 5a,b; SI Fig. S11a,b).

In contrast to the rate of daytime transpiration, changes in nighttime plant water use had a minimal impact on diel variation in aqueous mass of both NH_4^+ and K^+. Nighttime transpiration increased nighttime mass influx, increased desorption and increased root uptake of both NH_4^+ and K^+, which resulted in a slightly smaller loss of aqueous mass during the daytime period and no change in aqueous mass during the nighttime period, relative to the Base Case scenario (Fig. 5c,d; SI Fig. S11c,d). Nighttime root-water release had no impact on mass influx and decreased total desorption and root uptake of both NH_4^+ and K^+, though it enhanced the rate of desorption and root uptake of these two cations during the nighttime period (Fig. 5c,d; SI Fig. S11c,d). These mass balance shifts with nighttime root-water release resulted in no change aqueous mass during the daytime period and a slight increase in aqueous mass during the nighttime period, relative to the Base Case scenario. No diel variation existed in any of the mass balance components with constant root-ward water flow (SI Fig. S12).

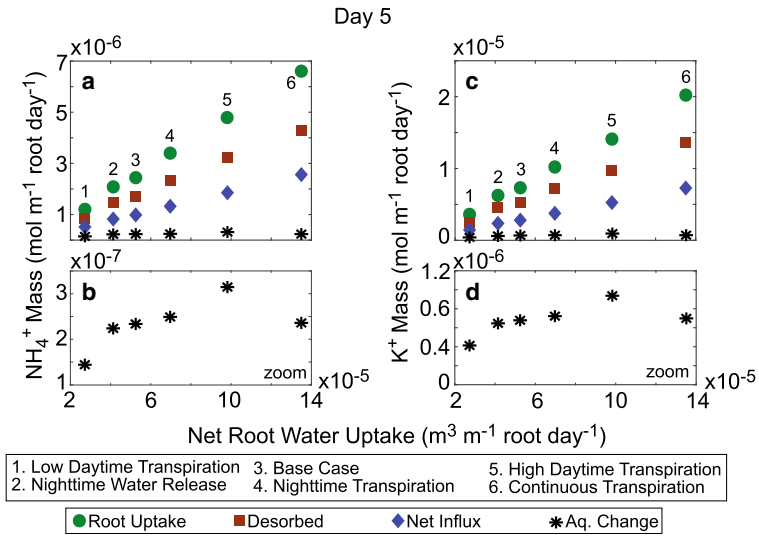

Fig. 4 Root uptake, desorption, net influx and change in aqueous mass for NH_4^+ (**a**-**b**) and K^+ (**c**-**d**) on day 5 of the simulation versus net root water uptake for the six different plant water use scenarios

In addition to shaping diel patterns in aqueous mass, the plant-driven water flow scenarios also affected day-to-night differences in peak concentrations and peak locations for the dissolved NH_4^+ and K^+ profiles (Fig. 3e,f; SI Fig. S4e,f). Figure 6 demonstrates that the difference between daytime and nighttime root water uptake controlled the day-to-night difference in peak concentrations for the dissolved NH_4^+ and K^+ profiles. With constant root-ward water flow, no difference existed between midday and midnight peak

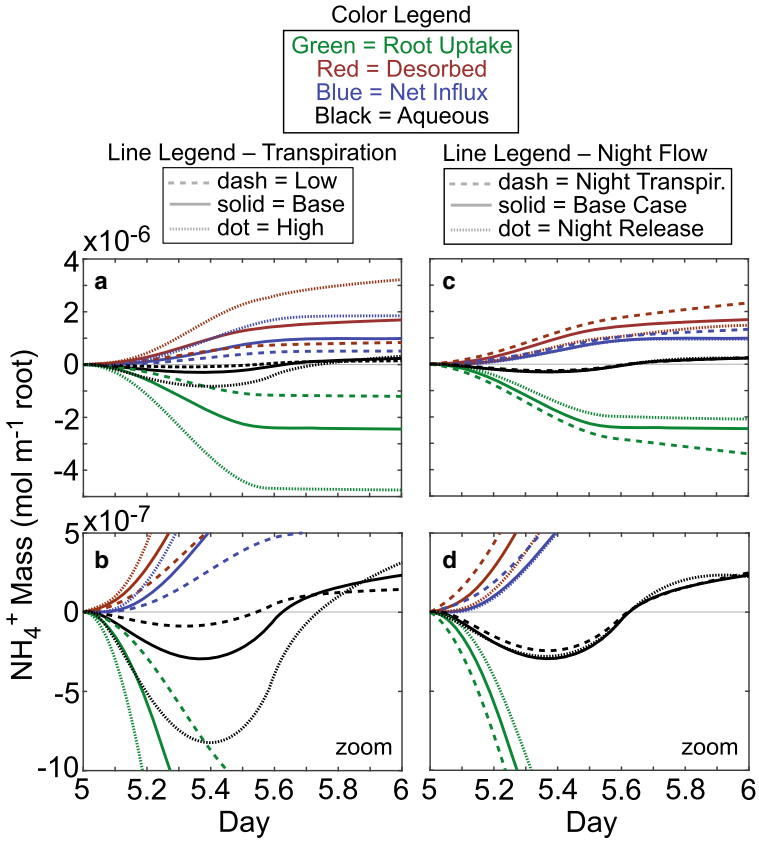

Fig. 5 Temporal change in NH_4^+ root uptake, desorption, net influx and aqueous mass during day 5 of the simulation for different rates of daytime transpiration coupled with no plant water use during the night (**a**-**b**) and for different nighttime plant water use scenarios (**c**-**d**)

concentrations for both NH_4^+ and K^+ (Fig. 6a,b). The two flow scenarios that decreased the day-to-night difference in root water uptake relative to the Base Case scenario (i.e., the scenario with a slower rate of daytime transpiration and the scenario with nighttime transpiration) resulted in smaller differences between midday and midnight peak concentrations, while the two flow scenarios that increased the day-to-night difference in root water uptake relative to the Base Case scenario (i.e., the scenario with a faster rate of daytime transpiration and the scenario with nighttime root-water release) resulted in larger differences between midday and midnight peak concentrations (Fig. 6a,b). A peak did not form for K^+ in the scenario with a fast daytime transpiration rate because the rate of K^+ delivery to the root exceeded the rate of K^+ root uptake (SI Fig. S4).

Previous results focused on Day 5 of the simulation. Figure 7 shows peak concentrations for the dissolved NH_4^+ and K^+ profiles at midnight over 30 simulated days for the six different flow scenarios. Peak concentrations for both dissolved cations initially increased at a rapid rate up until roughly day 5, at which point in time, peak concentrations in most of the flow scenarios continued to increase, but at a slower rate. Clear exceptions to this pattern were the flow scenarios with a high rate of daytime transpiration and with a constant root-ward water flow. With a high rate of daytime transpiration, peak concentrations for the dissolved NH_4^+ and K^+ profiles continued to increase between days 5 and 15, but then began to decrease after day 15 (Fig. 7a,b). With constant root-ward water flow, peak concentrations for the dissolved NH_4^+ and K^+ profiles reached their maximum value before day 5 and then continuously decreased with time (Fig. 7a,b).

Discussion

The model produced dissolved concentration profiles for Ca^{2+}, Mg^{2+}, Na^+ and NO_3^- that align with results from previous empirical and modeling studies (Lorenz et al. 1994; Barber 1995; Tinker and Nye 2000; Hinsinger et al. 2003; Nowack et al. 2006); low-demand cations (Ca^{2+}, Mg^{2+} and Na^+) accumulated against the root and nitrate concentrations decreased near the root. However, inclusion of competitive cation exchange generated non-monotonic dissolved concentration profiles for NH_4^+ and K^+ within the rhizosphere that have not previously been reported. These non-monotonic profiles were not re-created through the use of a sorption isotherm, demonstrating that they were generated due to competitive ion exchange. Previous modeling studies that have considered competitive ion exchange have generated similar non-monotonic concentration profiles for Ca^{2+} (Nietfeld and Prenzel 2015) and for phosphate, an anion (PO_4^{3-}) (Geelhoed et al. 1999; Nowack et al. 2006). In the Nietfeld and Prenzel (2015) study, Ca^{2+} was in low supply relative to plant demand, and therefore did not accumulate against the root. It was displaced from the soil via competitive interactions with aluminum (Al^{3+}), which in turn was controlled by pH-driven precipitation/dissolution reactions for aluminum hydroxide minerals. Mechanisms of formation for non-monotonic dissolved PO_4^{3-}profiles were related to interactions with root carbon exudates (e.g. citrate competitively desorbs phosphate, Geelhoed et al. 1999) that were diffusing away from the root as phosphate was transported toward the root with a constant water flow. These examples, as well as our modeling results, demonstrate how inclusion of reactive transport processes within the rhizosphere, such as competitive ion exchange, can alter nutrient availability and generate complex and dynamic solute concentration patterns that otherwise would not be reproduced. In the case of phosphorous, autoradiographs from empirical studies conducted with ^{33}P confirm that such non-monotonic profiles do develop within the rhizosphere (Hübel and Beck 1993).

A non-monotonic dissolved concentration profile with peak concentrations exceeding those in background soil solution indicates that reaction processes within the rhizosphere have increased the amount of that solute available for biological uptake — plant or microbial. Simulations conducted for this study demonstrated that root uptake of NH_4^+ and K^+ increased as more NH_4^+ and K^+ was competitively desorbed from the soil exchanger, which was directly coupled to the development of non-monotonic concentration profiles (i.e., compare profiles in Fig. 3e,f and SI Fig. S3e,f with plant uptake in Fig. 4). The model did not include microbial processes, but the development of non-monotonic concentration profiles could notably alter microbial activity within the rhizosphere, particularly if peak concentrations for key nutrients, such as NH_4^+ and PO_4^{3-}, spatially overlap with each other and with organic carbon exuded by plant roots (Dakora and Phillips 2002). In this study, the spatial location of peak dissolved NH_4^+ and K^+ concentrations were altered by

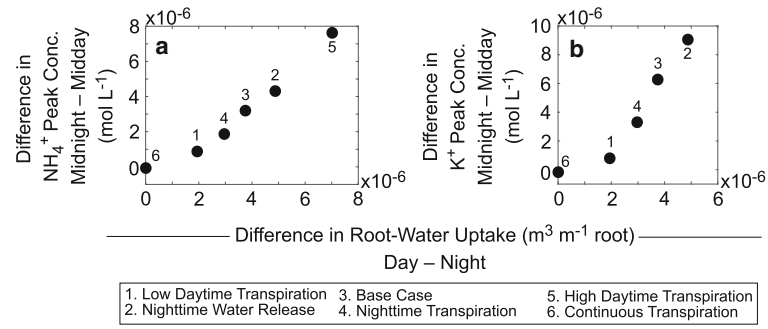

Fig. 6 Difference between midnight and midday peak concentrations for the dissolved NH_4^+ (**a**) and K^+ (**b**) profiles versus the difference between daytime and nighttime root water uptake for the six different plant water use scenarios. A peak did not form for K^+ in the high daytime transpiration scenario (see SI Fig. S4e)

changes in the cation exchange capacity (CEC) of the soil, with lower CEC pushing the peaks radially further from the root (Fig. 3a and SI Fig. S4a), and by nighttime water flow patterns, with nighttime transpiration pulling the peaks radially closer to the root and nighttime root-water release pushing the peaks radially further from the root (Fig. 3f and SI Fig. S4f).

We hypothesized that with competitive cation exchange, mass-flow delivery of cations to the root and subsequent accumulation of low-demand cations against the root would increase the availability of NH_4^+ and K^+ in the rhizosphere because accumulated cations would outcompete NH_4^+ and K^+ for sorption sites. Figure 4 indicates that this hypothesis was correct. Total water uptake by the root (i.e., root-ward water flow) controlled not only the net influx of NH_4^+ and K^+ into the rhizosphere domain, but also desorption of NH_4^+ and K^+ from the soil exchanger, and thus, net root-ward water flow controlled root uptake of these two cations.

Figure 4 has two implications. The first is that via the simulated processes, a plant-facilitated increase in root-ward water flow can stimulate the release of NH_4^+ and K^+ from the soil exchanger, increasing rhizosphere availability of these two solutes. Sensitivity tests illustrated that changes in plant water use had a larger impact on root uptake of NH_4^+ and K^+ than did changes in the Michaelis-Menten kinetic parameters for NH_4^+ and K^+ root uptake (i.e., compare Fig. 5 and SI Fig. S11 to SI Fig. S7 and S8). This sensitivity to plant-driven flow supports the body of literature arguing that plant control of water use, both rates of daytime transpiration and nighttime water use (i.e., nighttime transpiration and nighttime root-water release), can modify nutrient availability within the rhizosphere and alter plant nutrient uptake (e.g., Snyder et al. 2008; Cramer et al. 2009; Cardon et al. 2013; Cernusak et al. 2011; Matimati et al. 2014; Graciano et al. 2016).

The second implication of Fig. 4 is that simulation of diel plant water use was not needed for capturing total mass availability and root uptake of NH_4^+ and K^+ (in the absence of soil microbes) since net root-water uptake controlled these responses. Instead, diel plant water use altered the spatial and temporal dynamics of dissolved concentration profiles within the rhizosphere. Therefore, simulation of diel plant water use may not be necessary in studies focused on net root uptake of solutes that are not notably processed and altered by rhizosphere soil

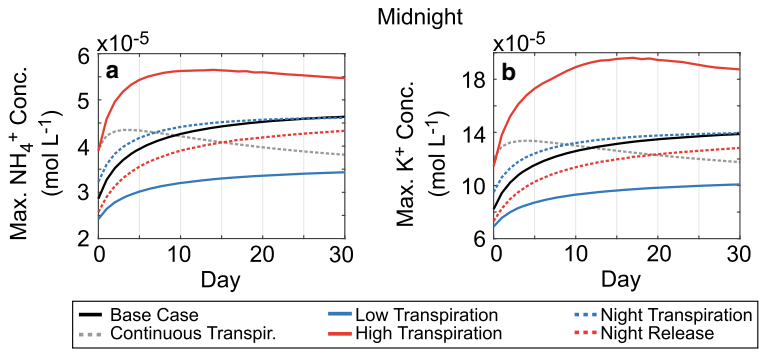

Fig. 7 Midnight peak concentrations for the dissolved NH_4^+ (**a**) and K^+ (**b**) profiles versus simulated time for the six different plant water use scenarios

microbes. The Yakirevich et al. (1994) investigation discussed in the Introduction is an example of such a study. It was focused on K^+ uptake by root systems growing in saline soils and simulated competitive cation exchange but not diel plant water use. For solutes like K^+, the spatial and temporal dynamics of dissolved rhizosphere concentrations may not markedly influence net root uptake. However, for solutes that are notably processed and altered by rhizosphere soil microbes, such as NH_4^+, simulation of diel plant water use is likely necessary. For these types of solutes, the spatial and temporal dynamics of dissolved rhizosphere concentrations could markedly alter net root uptake.

Cardon and Gage (2006) reasoned that temporal variation in resource availability in the rhizosphere driven by diel plant water use and root release of organic carbon could influence microbial processing of soil organic matter and thus alter root nitrogen uptake. In carbon-rich but nitrogen-poor conditions, soil microbes will produce long-lived exoenzymes that attack soil organic matter and release mineral nutrients. Cardon and Gage envisioned carbon rich conditions developing during the night when plant water use ceases and carbon from the root diffuses outward into the rhizosphere. The exoenzymes produced during the night would continue attacking soil organic matter during the day when plants transpire and root-ward water flow can deliver the released mineral nutrients (i.e., nitrogen) to the root. Whether the simulated temporal and spatial dynamics in dissolved NH_4^+ concentrations in this study stimulate or diminish microbial attack on soil organic matter is not clear. But these simulated dynamics indicate that studies focused on elucidating interactions between physical, chemical, plant and microbial processes within the rhizosphere should incorporate both competitive cation exchange and diel plant water use. Diel changes in NH_4^+ aqueous mass (Fig. 5), day-to-night differences in peak dissolved NH_4^+ concentrations (Fig. 6), day-to-night differences in the radial location of peak dissolved NH_4^+ concentrations (Fig. 3e,f), and longer-term trends in peak dissolved NH_4^+ concentrations (Fig. 7a), all driven by variations in plant water use, could meaningfully influence nutrient cycling within the rhizosphere.

The model developed for this study included two processes often neglected in rhizosphere and plant nutrient-uptake simulations — competitive cation exchange and diel plant water use — and results indicate that these two processes distinctly influenced the availability of NH_4^+ and K^+, as well as the spatial and temporal dynamics of dissolved NH_4^+ and K^+ profiles within the rhizosphere. However, the rhizosphere is an incredibly complex physical, biological and geochemical system, and presently, no model, including the one used in this study, completely represents this complexity. Some important simplifications made in the model used for this study include:

1) Root nutrient uptake was simulated as a purely active process. The model did not simulate the linear relationship that can exist between root nutrient uptake and solute concentrations when solute concentrations are elevated, i.e., passive uptake through ion channels (Marschner 1995). Inclusion of passive uptake would decrease cation build up near the root and, thus, would decrease competitive desorption of NH_4^+ and K^+ and decrease peak concentrations for the dissolved NH_4^+ and K^+ profiles. However, low-demand cations do accumulate near roots even when concentrations reach the point at which passive uptake occurs (e.g., milli-molar concentrations; Youssef and Chino 1987), and thus, inclusion of this process in the model would not eliminate the occurrence of non-monotonic profiles. Further, the simulated competitive displacement of NH_4^+ and K^+ from the soil exchanger by Ca^{2+}, Mg^{2+} and Na^+ required active root uptake. Passive root uptake operating alone would not enable Ca^{2+}, Mg^{2+} and Na^+ to accumulate against the root.
2) Root uptake of a given ion was influenced only by the concentration of that ion, synergistic and antagonistic interactions between ions on rates of root uptake were not considered. The Yakirevich et al. (1994) study discussed in the Introduction included the antagonistic effect that Na^+ can have on rates of K^+ uptake by the root. In sensitivity tests, this antagonistic interaction influenced modeled rates of K^+ uptake to the same extent that changing the Michaelis-Menten kinetic parameters for K^+ root uptake did. In the present study, the availability and dissolved concentration profiles of NH_4^+ and K^+ were largely insensitive to changes in the kinetic parameters describing rates of root nutrient uptake (Fig. 3c,d and SI Fig. S4c,d), and thus, we assume that inclusion of these types of interactions would minimally alter the simulation results.
3) Cation exchange capacity of the soil was constant. Cation exchange capacity is a function of the clay and organic carbon content of soil (Appelo and

Postma 2005). In the rhizosphere, organic carbon exuded by plant roots can increase CEC (Collignon et al. 2011). Inclusion of the impact that root exudates have on soil cation exchange capacity would increase CEC near the root, enhancing the opportunity for competitive displacement of NH_4^+ and K^+ near the root.

4) Microbes, protozoa and fungi, which can influence nutrient availability and plant growth (e.g., Bonkowski 2004) were not included. As mentioned earlier in the *Discussion* section, inclusion of these biological components would likely minimally influence simulated availability and concentration patterns for K^+, but could markedly alter availability and concentration patterns of NH_4^+.
5) The root did not grow and access new soil volumes over time (e.g., Kim et al. 1999). Figure 7 shows that peak concentrations for the dissolved NH_4^+ profiles initially increased with time and began to stabilize after five days. Thus, if roots grew slowly enough such that they spent at least five days within a given soil volume, then we assume that the simulated responses would not markedly change. However, if roots grew faster and moved through soil volumes in less than five days, then we assume that they would, by the simulated processes, access less NH_4^+ and K^+.
6) The model employed a single-root approach, which assumes that neighboring roots do not influence each other or compete with each other for water and solutes. This simplistic representation allowed for a straightforward examination of interactions between the simulated physical, chemical and plant-driven processes, and, ideally, the phenomena explored and characterized in this work can be incorporated into more complex root-rhizosphere models that more accurately represent root systems of varying architecture growing in heterogeneous soil environments (e.g., Doussan et al. 2003; Couvreur et al. 2012; Dunbabin et al. 2013).

Conclusions

The rhizosphere is physically, geochemically and biologically complex; no model currently captures all of this complexity. The model developed for this study investigated two processes often neglected in rhizosphere and plant-nutrients models: competitive soil cation exchange and diel plant-water use. Results demonstrated that these processes affected total availability of NH_4^+ and K^+ and influenced the spatial and temporal dynamics of dissolved NH_4^+ and K^+ concentration profiles in the rhizosphere. Competitive cation exchange enabled root-ward solute transport of low-demand cations (Mg^{2+}, Ca^{2+} and Na^+) to increase the availability of NH_4^+ and K^+, both high-demand cations; accumulation of Mg^{2+}, Ca^{2+} and Na^+ against the root facilitated competitive displacement of NH_4^+ and K^+ from the soil exchanger. NH_4^+ and K^+ desorption increased as net root water uptake increased because net root water uptake controlled the total flux of cations into the rhizosphere domain, and thus controlled the build-up of Mg^{2+}, Ca^{2+} and Na^+ against the root. This interaction presents a mechanism by which net plant water use can alter NH_4^+ and K^+ availability in the rhizosphere, beyond that due to simply increasing mass flux of NH_4^+ and K^+ into the soil domain. Diel plant water use influenced rhizosphere concentration patterns for NH_4^+ and K^+, which can have implications for rhizosphere nutrient cycling. Diel variation in NH_4^+ and K^+ aqueous mass was controlled by the strength of the daytime transpiration rate, spatial location of dissolved NH_4^+ and K^+ concentration peaks were controlled by nighttime plant water use, and day-to-night differences in the concentration of the dissolved NH_4^+ and K^+ peaks were controlled by the day-to-night difference in plant water use. Given these results, future models designed to elucidate interactions between physical, chemical, plant and microbial processes within the rhizosphere should include both competitive cation exchange and diel plant water use.

Acknowledgments This material is based upon work supported by the U.S. Department of Energy, Office of Science, Office of Biological & Environmental Research Terrestrial Ecosystem Science program under Award Number DE-SC0008182 to Z.G.C. and R.B.N. We thank Ed Rastetter for stimulating discussions that helped inform our thinking about the rhizosphere; Danyang Su and Mingliang Xie for their help with the MIN3P code; and Steve Burges, Maciej Zwieniecki and three anonymous reviewers for input that improved the manuscript.

References

Allison JD, Brown DS, Novo-Gradac KJ (1991) MINTEQA2/ PRODE- FA2, A geochemical assessment model for environmental systems, version 3.0, users's manual, EPA/600/3–91/021, Environ. Res. Lab., U.S. Environ. Prot. Agency, Washington, D. C

Appelo CAJ, Postma D (2005) Geochemistry, groundwater and pollution, 2nd edn. A.A. Balkema Publishers, Leiden, The Netherlands

Balland J, Pollacco JAP, Arp PA (2008) Modeling soil hydraulic properties for a wide range of soil conditions. Ecol Model 219:300–316

Barber SA (1995) Soil nutrient bioavailability: a mechanistic approach, 2nd edn. John Wiley & Sons, New York, USA

Bonkowski M (2004) Protozoa and plant growth: the microbial loop in soil revisited. New Phytol 162:617–631

Botella MA, Cerda A, Lips SH (1994) Kinetics of NO_3- and NH_4^+ uptake by wheat seedlings. Effect of salinity and nitrogen source J Plant Physiol 144:53–57

Bouldin DR (1989) A multiple ion uptake model. J Soil Sci 40: 309–319

Brady NC, Weil RR (2002) The nature and properties of soils, 13th edn. Prentice Hall, New Jersey, USA

Breeuwsma A, Wösten JHM, Vleeshouwer JJ, van Slobbe AM, Bouma J (1986) Derivation of land qualities to assess environmental problems from soil surveys. Soil Sci Soc Am J 50: 186–190

Brook GA, Folkoff ME, Box EO (1983) A world model of soil carbon dioxide. Earth Surf Process Landf 8:79–88

Caldwell MM, Richards JH (1989) Hydraulic lift: water efflux from upper roots improves effectiveness of water uptake by deep roots. Oecologia 79:1–5

Cardon ZG, Gage DJ (2006) Resource exchange in the rhizosphere: molecular tools and the microbial perspective. Annu Rev Ecol Evol Syst 37:459–488

Cardon ZG, Stark JM, Herron PM, Rasmussen JA (2013) Sagebrush carrying out hydraulic lift enhances surface soil nitrogen cycling and nitrogen uptake into inflorescences. Proc Natl Acad Sci U S A 110:18988–18993

Carrayrou J, Hoffmann J, Knabner P, Kräutle C, de Dieuleveult C, Erhel J, Van der Lee J, Lagneau V, Mayer KU, MacQuarrie KTB (2010) Comparison of numerical methods for simulating strongly nonlinear and heterogeneous reactive transport problems – the MoMaS benchmark case. Comput Geosci 14: 483–502

Cernusak LA, Winter K, Turner BL (2011) Transpiration modulates phosphorus acquisition in tropical tree seedlings. Tree Physiol 31:878–885

Chapin FS, Matson PA, Mooney HA (2002) Principles of terrestrial ecosystem ecology. Springer Verlag, New York

Claassen N, Syring KM, Jungk A (1986) Verification of a mathematical-model by simulating potassium uptake from soil. Plant Soil 95:209–220

Collignon C, Calvaruso C, Turpault M-P (2011) Temporal dynamics of exchangeable K, Ca and Mg in acidic bulk soil and rhizosphere under Norway spruce (*Picea abies* karst.) and beech (*Fagus sylvatica* L.) stands. Plant Soil 349(1–2):355–366

Coners H, Leuschner C (2005) In situ measurement of fine root water absorption in three temperate tree species—temporal variability and control by soil and atmospheric factors. Basic Appl Ecol 6(4):395–405

Couvreur V, Vanderborght J, Javaux M (2012) A simple three-dimensional macroscopic root water uptake model based on the hydraulic architecture approach. Hydrol Earth Syst Sci 16(8):2957–2971

Cramer MD, Hawkins H-J, Verboom AG (2009) The importance of nutritional regulation of plant water flux. Oecologia 161: 15–14

Dakora F, Phillips D (2002) Root exudates as mediators of mineral acquisition in low-nutrient environments. Plant Soil 245:35–47

Dawson TE, Burgess SSO, Tu KP, Oliveira RS, Santiago LS, Fisher JB, Simonin KA, Ambrose AR (2007) Nighttime transpiration in woody plants from contrasting ecosystems. Tree Physiol 27:561–575

Domec J-C, Warren J, Meinzer F, Brooks J, Coulombe R (2004) Native root xylem embolism and stomatal closure in stands of Douglas-fir and ponderosa pine: mitigation by hydraulic redistribution. Oecologia 141(1):7–16

Domenico PA, Schwartz FW (1998) Physical and chemical hydrogeology, 2nd edn. John Wiley & Sons, New York, USA

Doussan C, Pages L, Pierret A (2003) Soil exploration and resource acquisition by plant roots: an architectural and modelling point of view. Agron 23(5–6):419–431

Dunbabin VM, Postma JA, Schnepf A, Pages L, Javaux M, Wu L, Leitner D, Chen YL, Rengel Z, Diggle AJ (2013) Modelling root–soil interactions using three–dimensional models of root growth, architecture and function. Plant Soil 372:93–124

Forster MA (2014) How significant is nocturnal sap flow? Tree Physiol 34:757–764

Geelhoed JS, Van Riemsdijk WH, Findenegg GR (1999) Simulation of the effect of citrate exudation from roots on the plant availability of phosphate adsorbed on goethite. Eur J Soil Sci 50:379–390

Gelhar LW, Welty C, Rehfeldt KR (1992) A critical review of data on field-scale dispersion in aquifers. Water Resour Res 28: 1955–1974

Graciano C, Faustino LI, Zwieniecki MA (2016) Hydraulic properties of *Eucalyptus grandisin* response to nitrate and phosphate deficiency and sudden changes in their availability. J Plant Nutr Soil Sci 179:303–309

Hinsinger P, Plassard C, Tang C, Jaillard B (2003) Origins of root-mediated pH changes in the rhizosphere and their responses to environmental constraints: a review. Plant Soil 248:43–59

Hübel F, Beck B (1993) In-situ determination of the P-relations around the primary root of maize with respect to inorganic and phytate-P. Plant Soil 157:1–9

Ishikawa C, Bledsoe C (2000) Seasonal and diurnal patterns of soil water potential in the rhizosphere of blue oaks: evidence for hydraulic lift. Oecologia 125(4):459–465

Jellali S, Diamantopoulos E, Kallali H, Bennaceur S, Anane M, Jedidi N (2010) Dynamic sorption of ammonium by sandy soil in fixed bed columns: evaluation of equilibrium and non-equilibrium transport processes. J Environ Manag 91:897–905

Kim TK, Silk WK, Cheer AY (1999) A mathematical model for pH patterns in the rhizospheres of growth zones. Plant Cell Environ 22:1527–1538

Lima AMN, Neves JCM, Silva IR, Leite FP (2005) Cinética de absorção e eficiência nutricional de K^+, Ca^{2+} e Mg^{2+} em plantas jovens de quatro clones de eucalipto. Revista Brasileira de Ciência do Solo (Brazilian Journal of Soil Science) 29:903–909

Lin W, Kelly M (2010) Nutrient uptake estimates for woody species as described by the NST 3.0, SSAND, and PCATS mechanistic nutrient uptake models. Plant Soil 335:199–212

Lorenz SE, Hamon RE, McGrath SP (1994) Differences between soil solutions obtained from rhizosphere and non-rhizosphere soils by water displacement and soil centrifugation. Euro J Soil Sci 45:431–438

Luster J, Göttlein A, Nowack B, Sarret G (2009) Sampling, defining, characterising and modeling the rhizosphere—the soil science tool box. Plant Soil 321:457–482

Marrero TR, Mason EA (1972) Gaseous diffusion coefficients. J Phys Chem Ref Data 1:3–118. doi:10.1063/1.3253094

Marschner H (1995) Mineral nutrition of higher plants, 2nd edn. Academic Press, San Diego, California, USA

Marty NCM, Bildstein O, Blanc P, Claret F, Cochepin B, Gaucher EC, Jacques D, Lartigue J-E, Liu S, Mayer KU, Meeussen JCL, Munier I, Pointeau I, Su D, Steefel C (2015) Benchmarks for multiocomponent reactive transport across a cement/clay interface. Comput Geosci 19(3):635–653

Matamala R, Stover DB (2013) Introduction to a virtual special issue: modeling the hidden half–the root of our problem. New Phytol 200:939–942

Matimati I, Verboom GA, Cramer MD (2014) Nitrogen regulation of transpiration controls mass-flow acquisition of nutrients. J Exp Bot 65:159–168

Mayer KU, MacQuarrie KTB (2010) Solution of the MoMaS reactive transport benchmark with MIN3P - model formulation and simulation results. Comput Geosci 14:405–419

Mayer KU, Frind EO, Blowes DW (2002) Multicomponent reactive transport modeling in variably saturated porous media using a generalized formulation for kinetically controlled reactions. Water Resour Res 38:1174–1195

Meinzer F, Brooks J, Bucci S, Goldstein G, Scholz F, Warren J (2004) Converging patterns of uptake and hydraulic redistribution of soil water in contrasting woody vegetation types. Tree Physiol 24(8):919–928

Meinzer F, Warren J, Brooks J (2007) Species-specific partitioning of soil water resources in an old-growth Douglas-fir-western hemlock forest. Tree Physiol 27(6):871–880

Millington RJ, Quirk JP (1959) Permeability of porous media. Nature 183:387–388

Neumann RB, Cardon ZG (2012) The magnitude of hydraulic redistribution by plant roots: a review and synthesis of empirical and modeling studies. New Phytol 194:337–352

Neumann RB, Cardon ZG, Teshera-Levye J, Rockwell FE, Zwieniecki MA, Holbrook NM (2014) Modelled hydraulic redistribution by sunflower (*Helianthus annuus* L.) matches observed data only after including night-time transpiration. Plant Cell Environ 37:899–910

Nietfeld H, Prenzel J (2015) Modeling the reactive ion dynamics in the rhizosphere of tree roots growing in acid soils. I. Rhizospheric distribution patterns and root uptake of Mb cations as affected by root-induced pH and Al dynamics. Ecol Model 307:48–65

Norby RJ, Jackson RB (2000) Root dynamics and global change: seeking an ecosystem perspective. New Phytol 147(1):3–12

Nowack B, Mayer KU, Oswald SE, van Beinum W, Appelo CAJ, Jacques D, Seuntjens P, Gérard F, Jaillard B, Schnepf A, Roose T (2006) Verification and intercomparison of reactive transport codes to describe root-uptake. Plant Soil 285:305–321

Rasouli P, Steefel CI, Mayer KU, Rolle M (2015) Benchmarks for multicomponent diffusion and electrochemical migration. Comput Geosci 19(3):523–533

Schaap MG, Leij FJ (2000) Improved prediction of unsaturated hydraulic conductivity with the Mualem – van Genuchten model. Soil Sci Soc Am J 64:843–851

Snyder K, James J, Richards J, Donovan L (2008) Does hydraulic lift or nighttime transpiration facilitate nitrogen acquisition? Plant Soil 306:159–166

Steefel CI, Yabusaki SB, Mayer KU (2015) Reactive transport benchmarks for subsurface environmental simulation. Comput Geosci 19:439–443

Tinker PB, Nye PH (2000) Solute movement in the rhizosphere. Oxford University Press, New York, USA

Waisel Y, Eshel A, Kafkafi U (1991) Plant roots the hidden half, 3rd edn. Marcel Dekker, New York

Wösten J, Van Genuchten MT (1988) Using texture and other soil properties to predict the unsaturated soil hydraulic functions. Soil Sci Soc Am J 52:1762–1770

Yakirevich A, Sorek S, Silberbush M (1994) K^+ uptake by root systems grown in soil under salinity: II. Sensitivity analysis. Transp. Porous Media 14:123–141

Youssef A, Chino M (1987) Studies on the behavior of nutrients in the rhizosphere I: establishment of a new rhizobox system to study nutrient status in the rhizosphere. J Plant Nutr 10:1185–1195